UC Davis

UC Davis Previously Published Works

Title

His74 conservation in the bilin reductase PcyA family reflects an important role in protein-substrate structure and dynamics

Permalink

https://escholarship.org/uc/item/3kt1q993

Journal

Archives of Biochemistry and Biophysics, 537(2)

ISSN

0003-9861

Authors

Kabasakal, Burak V

Gae, David D

Li, Jie

et al.

Publication Date

2013-09-01

DOI

10.1016/j.abb.2013.07.021

Peer reviewed

eScholarship.org Powered by the California Digital Library
University of California

Archives of Biochemistry and Biophysics xxx (2013) xxx–xxx

Contents lists available at ScienceDirect

Archives of Biochemistry and Biophysics

journal homepage: www.elsevier.com/locate/yabbi

His74 conservation in the bilin reductase PcyA family reflects an important role in protein-substrate structure and dynamics

Burak Kabasakal[a,1], David D. Gae[d,1], Jie Li[c,2], J. Clark Lagarias[b], Patrice Koehl[c], Andrew J. Fisher[a,b,*]

[a] Department of Chemistry, University of California, One Shields Avenue, Davis, CA 95616, United States
[b] Department of Molecular and Cellular Biology, University of California, One Shields Avenue, Davis, CA 95616, United States
[c] Genome Center, University of California, One Shields Avenue, Davis, CA 95616, United States
[d] Biophysics Graduate Program, University of California, One Shields Avenue, Davis, CA 95616, United States

ARTICLE INFO

Article history:
Received 26 June 2013
Available online xxxx

Keywords:
Phycocyanobilin
Biliverdin
Ferredoxin
MD simulations
Oxidoreductase

ABSTRACT

Phycocyanobilin:ferredoxin oxidoreductase (PcyA) catalyzes the proton-coupled four-electron reduction of biliverdin IXα's two vinyl groups to produce phycocyanobilin, an essential chromophore for phytochromes, cyanobacteriochromes and phycobiliproteins. Previous site directed mutagenesis studies indicated that the fully conserved residue His74 plays a critical role in the H-bonding network that permits proton transfer. Here, we exploit X-ray crystallography, enzymology and molecular dynamics simulations to understand the functional role of this invariant histidine. The structures of the H74A, H74E and H74Q variants of PcyA reveal that a "conserved" buried water molecule that bridges His74 and catalytically essential His88 is not required for activity. Despite distinct conformations of Glu74 and Gln74 in theH74E and H74Q variants, both retain reasonable activity while the H74A variant is inactive, suggesting smaller residues may generate cavities that increase flexibility, thereby reducing enzymatic activity. Molecular dynamic simulations further reveal that the crucial active site residue Asp105 is more dynamic in H74A compared to wild-type PcyA and the two other His74 variants, supporting the conclusion that the Ala74 mutation has increased the flexibility of the active site.

© 2013 Elsevier Inc. All rights reserved.

Introduction

Phytobilins are heme-derived linear tetrapyrroles that perform important functions in oxygenic photosynthetic organisms including green plants, cyanobacteria and red algae [1,2]. When attached to proteins (biliproteins) via thioether linkages to cysteine residues, phytobilins function as light sensors and as light-harvesting antennae. Phytobilins attached to phytochromes [3,4] function to regulate photomorphogenesis in plants [5]. Cyanobacteria, red algae, and cryptomonad algae also utilize phytobilins in the light-harvesting phycobilisomes that absorb light and transfer the captured energy to the chlorophylls in the photosynthetic reaction centers [6,7]. Since biliproteins are necessary both for energy capture and for adaptation to the light environment, production of these linear tetrapyrroles is critical to photoautotrophic organisms in which they are present.

The linear tetrapyrrole phycocyanobilin (PCB),[3] comprising the chromophores of algal phytochromes and core phycobiliprotein antennae of cyanobacteria and red algae, is synthesized by the enzyme phycocyanobilin:ferredoxin oxidoreductase (PcyA; EC 1.3.7.5). A member of the ferredoxin-dependent biliverdin reductase (FDBR) family [8], PcyA catalyzes the multi-step reduction of biliverdin IXα(BV) to produce 3*Z*/3*E*-phycocyanobilin (3*Z*/3*E*-PCB). PcyA mediates four one-electron transfers to BV – a ferredoxin-dependent reaction that proceeds via two radical intermediates (first and third electron transfer) [9] and a stable two-electron reduced intermediate 18^1,18^2-dihydrobiliverdin (DHBV) to yield PCB (Scheme 1) [8,10]. DHBV is not detected under steady state conditions, suggesting that this intermediate remains bound to the enzyme until the endovinyl reduction is complete [8,10]. Although the three dimensional structure of PcyA has been extensively studied crystallographically [11–13], a mechanistic understanding of the structural basis for PcyA's reduction regiospecificity remains unclear.

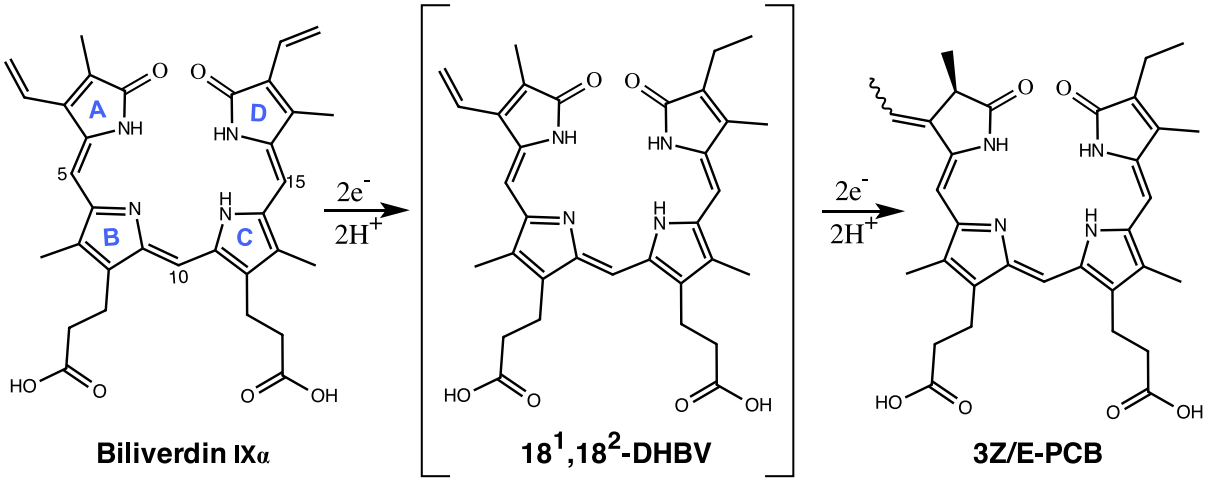
* Corresponding author. at: Department of Chemistry, University of California, One Shields Avenue, Davis, CA 95616, United States. Fax: +1 530 752 8995.
E-mail addresses: fisher@chem.ucdavis.edu, ajfisher@ucdavis.edu (A.J. Fisher).

[1] These authors contributed equally to this work.

[2] Protein coordinates have been deposited in the Protein Data Bank (IDs 4eoc, 4eod and 4eoe for the H74Q, H74E and H74A variants respectively).

[3] *Abbreviations used:* PcyA, phycocyanobilin:ferredoxin oxidoreductase; FDBR, ferredoxin-dependent bilin reductase; PCB, phycocyanobilin; BV, biliverdin IXα; DHBV, 18^1,18^2-dihydrobiliverdin IXα; Fd, ferredoxin; FNR, ferredoxin:NADP oxidoreductase; RMSD, root mean squared deviation.

0003-9861/$ - see front matter © 2013 Elsevier Inc. All rights reserved.
http://dx.doi.org/10.1016/j.abb.2013.07.021



Scheme 1.

With each electron transfer, a proton must be transferred to the bilin substrate [9,12,14]. Site directed mutagenesis has been a powerful tool to help identify residues that mediate this proton donation to the tetrapyrrole substrate. Previously, His88 and Asp105 (*Synechocystis* sp. PCC 6803 PcyA numbering) were shown to be critical for the reduction of both vinyl groups [14]. Crystal structures reveal that these residues interact in the absence of substrate, but move apart upon BV binding to interact with the bilin substrate [11,12,15]. In the substrate-free PcyA structure, the protonated imidazolium group of His88 is ion paired with the carboxylate side chain of Asp105. NMR studies suggest that an imidazolium proton/His88 is transferred to Asp105 upon substrate binding, resulting in a mostly charge-neutral pocket with bound BV [13]. Substitution of either residue with a non-proton-donating amino acid prevents transfer of a second electron thereby stabilizing the one-electron reduced BVH**.** radical [16]. In addition to D-ring exovinyl group reduction, His88 also plays a critical role in A-ring endovinyl reduction since the H88Q variant is unable to reduce the A-ring vinyl group of exogenous DHBV [12]. Re-protonation of H88 therefore appears necessary for endovinyl reduction.

The crystal structures of PcyA show that conserved residue His74 is H-bonded via a bridging water molecule to His88 suggesting that His74 plays a direct role in His88 re-protonation. Moreover, the buried water between His88 and His74 is present whether or not substrate is bound. Interestingly, exchange of His74 with other residues only capable of hydrogen bonding merely reduced the activity – i.e. H74Q, H74E and H74 N had 65%, 50% and 46% of wild-type PcyA activity, while the H74A variant was nearly inactive [14]. These data establish that His74 is not an essential proton donor, but implicate a role for this residue to position the bridging water molecule to mediate subsequent proton transfer to the reduced substrate.

The present work was undertaken to correlate the enzymatic activities of PcyA wild type and H74Q, H74E and H74A variants from the cyanobacterium *Synechocystis* sp. PCC 6803 with their corresponding X-ray crystal structures. Surprisingly, the presence of the bridging water is not correlated with the activity of the PcyA variant. While the presence of this bridging water in the H74A variant is apparently inconsistent with its role in proton transfer, a gap in the region near the Ala74 side-chain is observed in the H74A variant. We therefore performed molecular dynamics simulations of native PcyA as well as all three variants, H74Q, H74Q and H74A, in the presence of BV. These simulations reveal that the gap in the region near Ala74 in the H74A variant facilitates flipping of the conserved active site residue Asp105, leading to greater flexibility of BV in the active site. This increase of flexibility accounts for the reduced affinity of the substrate and the loss of activity for theH74A variant.

Materials and methods

Site-directed mutagenesis, expression and purification of Synechocystis PcyA

Synechocystis sp. PCC 6803 PcyA variants were generated from the wild type cloned into the expression vector pTYB12 (New England BioLabs, Ipswich, MA) using the QuikChange site-directed mutagenesis kit (Stratagene, La Jolla, CA). PCR primers used were: ***H74A_F,***CAGTTTCGCAAAATG**GCG**TTGGAGTTGGCCAAG; ***H74A_R,*** GTCAAAGCGTTTTAC**CGC**AACCTCAACCGGTTC; ***H74E_F,***CAGTTTCGC AAAATG**GAG**TTGGAGTTGGCCAAG; ***H74E_R,***GTCAAAGCGTTTTAC **C TC**AACCTCAACCGGTTC; ***H74Q_F,***CAGTTTCGCAAAATG**CA G**TTGGA GTTGGCCAAG; ***H74Q_R,***GTCAAAGCGTTTTAC**GTC**AACCTCA ACCG GTTC. All new clones, characterized by DNA sequencing (Davis Sequencing, Davis, CA), were transformed into *Escherichia coli* strain BL21-DE3 (Stratagene, La Jolla, CA) for protein expression. After lactose induction at 15 °C for 19 h, variant proteins were purified according to the IMPACT-CN protein purification protocol (New England BioLabs, Beverly, MA) with the following modifications. Cell lysis buffer consisted of 50 mM Tris–HCl, pH 8.0, 0.5 M NaCl, 0.25 mM EDTA and 0.1% (v/v) Triton-X 100 and column equilibration buffer consisted of 50 mM Tris–HCl, pH 8.0, 0.5 M NaCl, 0.25 mM EDTA. On-column cleavage was performed by addition of 50 mM 2-mercaptoethanol to column equilibration buffer (50 mM Tris–HCl, pH 8.0, 0.5 M NaCl, 0.25 mM EDTA) followed by incubation at 4 °C for 48 h. The cleaved protein was eluted with 35 mL of the buffer (50 mM Tris–HCl, pH 8.0, 0.5 M NaCl, 0.25 mM EDTA). The purified protein was subsequently dialyzed in 20 mM Tris–HCl, pH 8.0 for 24 h, followed by concentration using Amicon Ultra 10,000 MWCO centrifugal tubes (Millipore Corp, Billerica, MA) to approximately 15 mg/mL. Concentrated PcyA protein was stored at −80 °C.

PcyA end-point assay

NADPH (Cat. No. N-1630), ferredoxin:NADP$^+$ oxidoreductase (FNR) (Cat. No. F-0628), glucose oxidase (Cat. No. G6125) and catalase (Cat No. C-40) were purchased from Sigma–Aldrich. Bovine serum albumin (Cat. No. 100–018) was purchased from Boehringer-Mannheim. HPLC grade acetone, acetonitrile, formic acid and

UNCORRECTED PROOF

spectroanalytical grade glycerol were obtained from Fisher Scientific. Sep-Pak Light cartridges were obtained from Waters (Cat. No. WAT023501). Biliverdin IXα was prepared as described previously [9,13,17]. Recombinant *Synechocystis* sp. PCC7002 ferredoxin (Fd) was expressed and purified as described previously [12].

PcyA assays were performed under dim light. All buffers were vacuum-degassed prior to preparation. Reaction mixtures for standard assays were prepared in TKK buffer (25 mM TES-KOH pH 8.5, 100 mM KCl) containing 10 μM PcyA, 10 μM BV, 0.0025 U/ml FNR (3 nM final concentration), 10 μM ferredoxin, 10 μM bovine serum albumin, and an oxygen scavenging system (25 U/ml glucose oxidase, 100 mM glucose and 5 U/ml catalase). Reaction mixtures were incubated with stirring at 16 °C in septum-stoppered quartz cuvettes over which 99% pure N_2 was passed for 30 min in a thermostable cell holder. To control the reaction temperature and to mix the reaction mixture, a cell stirring module was used. Catalytic reaction was initiated by injecting 10 electron equivalents of NADPH (50 μM final concentration) into reaction mixtures in cuvettes using a gas-tight syringe. NADPH stock solutions were quantified using $\varepsilon_{340} = 6220\ M^{-1}\ cm^{-1}$. After 30 min, reaction products were analyzed with HPLC (Agilent Technologies 1100) after a cleanup process. The products were extracted and analyzed as follows: Bilin pigments were extracted/eluted using Waters C18 Sep-Pak Light cartridges followed by evaporation to dryness using a SpeedVac concentrator. The dry samples were dissolved in 10 μL of DMSO, diluted with 190 μL of HPLC mobile phase and filtered with 0.45 μm poly (tetrafluoroethylene) syringe filters prior to injection onto a 4.6 × 250 mm Phenomenex Ultracarb 5 μm ODS [14] reverse-phase column equipped with a 4.6 × 30 mm guard column of the same material. 50% acetone and 50% 20 mM formic acid (by volume) was used as the mobile phase and the flow rate was 0.6 mL. The eluate was monitored with an Agilent Technologies 1100 diode array detector at 650 nm. Elution order coming off the column was 3E-PCB, 18^1,18^2-DHBV, 3Z-PCB and BV, respectively.

Crystallization of synechocystis PcyA variants

Variant PcyA enzymes were crystallized by hanging drop vapor diffusion at 21 °C in 24-well Linbro plates with a drop size of 4 μL (2 μL protein + 2 μL precipitant solution) containing 15 mg/mL protein and 0.67 mM BV (1:1.25 M ratio (protein:BV)). Conditions that resulted in the best diffracting substrate-bound PcyA crystals were 1–1.25 M sodium citrate, 0.1–0.4 M NaCl in 0.1 M Tris HCl, pH 7.0. Crystal trials were set up under green safelight and stored in the dark. Primitive orthorhombic crystals grew in 1–2 weeks.

Diffraction data collection of Synechocystis PcyA

Individual PcyA crystals were sequentially transferred to Partone-N oil or a cryosolution containing 30% (v/v) ethylene glycol in mother liquor and flash frozen in liquid nitrogen. X-ray diffraction data from H74A was collected on beam line 9-2 while H74E and H74Q variants were collected on beam line 7-1 at the Stanford Synchrotron Radiation Lightsource (SSRL). Diffraction data were indexed and integrated with MOSFLM [18] or XDS [19]. Complete

Table 1
Data collection and refinement statistics.

PcyA variant	H74A	H74E	H74Q
X-ray source	SSRL BL 9-2	SSRL BL 7-1	SSRL BL 7-1
Wavelength (Å)	0.979	0.979	0.979
Space group	$P2_12_12$	$P2_12_12$	$P2_12_12$
a (Å)	71.21	70.57	70.40
b (Å)	95.78	95.19	94.88
c (Å)	42.91	42.73	42.57
Resolution (Å)	1.18 (1.21-1.18)	1.30 (1.33-1.30)	1.49 (1.53-1.49)
No. of reflections	260,503 (12,798)	251,259 (16,453)	163,726 (11,431)
No. of unique reflections	88,225 (4,616)	70,757 (4,572)	46,661 (3,356)
Completeness (%)	93.1 (67.0)	98.2 (97.2)	98.6 (96.2)
R_{merge}[a] (%)	2.9 (30.5)	4.6 (43.4)	3.0 (44.7)
I/σ	14.0 (2.4)	15.7 (3.3)	21.7 (2.7)
Refinement statistics			
Resolution (Å)	28.989-1.18	39.034-1.30	38.84-1.49
No. of reflections ($F \geqslant 0$)	83,812	67,204	44,307
R-factor[b] (%)	14.88	16.52	17.95
R-free[b] (%)	17.08	18.83	20.72
RMS bond length (Å)	0.011	0.012	0.012
RMS bond angle (°)	1.595	1.597	1.633
Ramachandran plot statistics			
Residues[c]	240	241	234
Most favorable regions (%)	97.9	97.9	97.0
Allowed regions (%)	2.1	2.1	3.0
Disallowed (%)	0.0	0.0	0.0
Asymmetric Unit Content			
Non-hydrogen protein atoms	2070	2067	1997
BV atoms	45	43	45
Waters	315	311	310
Chloride ions	3	2	2
RMSD to wild type (#cα's)	0.292 Å (217)	0.193 Å (218)	0.353 Å (222)
PDB ID	4eoe	4eod	4eoc

[a] $R_{merge} = [03A3_h\Sigma_i|I_h - I_{hi}|/\Sigma_h\Sigma_i I_{hi}]$ where I_h is the mean of I_{hi} observations of reflection h. Numbers in parenthesis represent highest resolution shell.
[b] *R*-factor and$R_{free} = \Sigma||F_{obs}| - |F_{calc}||/\Sigma|F_{obs}| \times 100$ for 95% recorded data (*R*-factor) or 5% of data (*R*-free). Numbers in parenthesis represent highest resolution shell.
[c] Number of non-proline and non-glycine residues used for calculation.

UNCORRECTED PROOF

data sets were collected to 1.18, 1.30 and 1.49 Å resolution for H74A, H74E and H74Q variant PcyA crystals, respectively. Table 1 displays all the data collection and refinement statistics.

Structure solution, model building and refinement

Structures were solved by Molecular Replacement using the wild-type *Synechocystis* PcyA structure (PDB ID: 2D1E) by PHASER in the CCP4 program suite [20]. Refinement was performed using REFMAC5 in the CCP4 program suite [21]. Model building was carried out with the molecular graphics program COOT [22]. The models were refined with final statistics of R_{factor} of 14.88%, 16.52% and 17.95% and R_{free} of 17.08% and 18.83%, 20.72% for H74A, H74E and H74Q variant proteins, respectively. The results for the final models are summarized in Table 1.

Molecular dynamics simulations

Molecular dynamics simulations were performed for wild-type PcyA and the three variants H74A, H74E and H74Q, using their X-ray structures as starting conformations (PDB code 2DIE for wild-type PcyA, and the structures determined in this study for the variants). All simulations were designed to mimic physiological conditions at neutral pH. Under these conditions and based on previous biochemical data, Glu76 and Asp105 are expected to be protonated (i.e. uncharged) in these structures. Indeed, we have shown previously using biochemistry, UV/VIS, EPR and NMR spectroscopy that Asp105 is protonated and transfers its proton to BV as part of the first electron transfer [12–14,16]. There is also evidence that Glu76 is protonated since it is required for D-ring reduction [23]. Asp105 and Glu76 were therefore protonated in all simulations reported in this paper. Additionally, His88 is assumed to be neutral. All other ionizable groups were assigned to their protonation state expected in solution at neutral pH.

AMBER ff99SB parameters [24] were used for amino acids and GAFF parameters were used for BV [25]. BV topology was created using the ANTECHAMBER program [26]. In addition, manual correction of C15-C16-C17-C18 carbons to cf-cc-cc-cd atom type was applied to maintain (quasi)planarity of the C and D rings, as the PARMCHK program failed to produce all improper and proper dihedrals for the highly symmetric BV system. PARMCHK program [26] was then rerun to check for all missing parameters of BV. The charges were derived based on AM1-BCC scheme [27]. Slight adjustments of the AM1-BCC charges were performed manually in order to maintain the same charge scheme for BV among all simulations.

A box of TIP3P water with 13 Å between the protein and the edge of the box was generated using tLeap [28]. Bound water molecules determined by X-ray crystallography were retained. Appropriate counter ions (Na^+ or Cl^-) were placed to obtain a neutral system. The system was step-wise minimized. Protein plus BV were fixed for 3000 steps of Conjugate Gradient (CG) minimization to relax the water molecules. Next the protein plus BV was minimized with 700 steps of CG, while fixing the water. A final minimization with 1000 steps of CG was carried out to relax the whole system. The MPI version of NAMD2.7 program [29] was used for the minimization process.

The system was heated incrementally by increasing the temperature from 10 to 298 K over 30 ps. It was further equilibrated for 120 ps at a constant pressure of 1 atm using Berendsen coupling method [30] and constant temperature of 298 K using the reassign-hold method [29]. During the entire equilibration procedure, the BV was restrained with a harmonic potential using a force constant of 2 kcal/mol/Å^2 in order to maintain the crystallographic configuration of BV. This was done to sample between BV conformations and catalytically important residues during the production run. At the production phase, BV restraints were released, temperature was maintained at 298 K with an external heat bath and 1 atm pressure was held constant using a Berendsen coupling method [30]. Periodic boundary conditions were applied throughout the simulations. Long range electrostatic interactions were treated with particle mesh Ewald [PME] method [31] and a switching function was employed between 9 and 12 Å to gradually reduce the electrostatics and van der Waals interactions [29] to zero. The*verlet* algorithm was used for time integration with a time step of 1 fs. Three independent simulations, each of sixty nanoseconds, were performed for each of the four proteins (wild-type PcyA and H74A, H74E and H74Q variants). Snapshots were collected every 10 ps during these simulations for later analysis.

Atomic root mean squared fluctuations (RMSF) over the simulations were computed using the following equation:

$$\mathrm{RMSF}(i) = \sqrt{\frac{1}{N}\sum_{j=1}^{N}\left(r_i^j - < r_i >\right)^2}$$

where r_i^j refers to the position of atom i at timeframe j, $\langle r_i \rangle$ is the mean position of the same atom i over the whole simulation, and the summation extends over all N timeframes considered. We com-

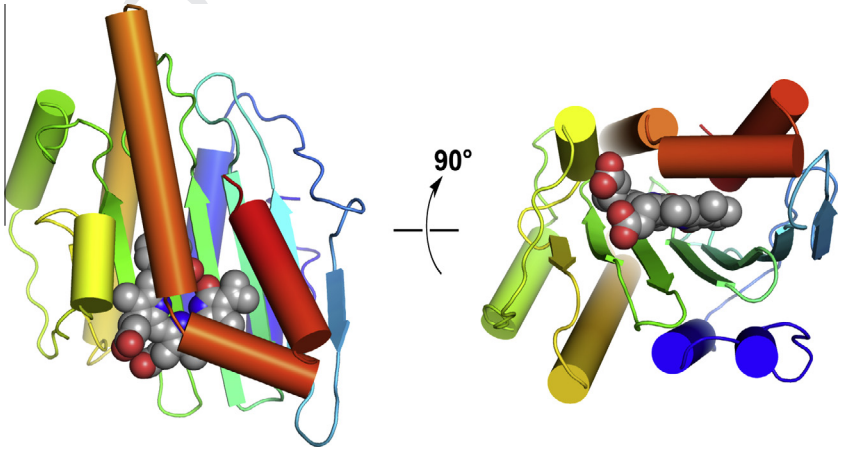


Fig. 1. Structure of the H74A variant with biliverdin bound (right view is rotated 90° about horizontal axis). The protein is colored with a rainbow spectrum starting with blue at the N-terminus and ending with red at the C-terminus. The biliverdin is shown as space filling model with gray-colored carbon atoms. Figs. 1–3 were generated by PyMol (www.pymol.org). (For interpretation of the references to color in this figure legend, the reader is referred to the web version of this article.)

CORRECTED PROOF

puted RMSF for individual atoms as well as averaged over residues in the neighborhood of BV.

Center of gravity was calculated for BV substrate over the simulations using the following equation:

$$\text{Center of gravity} = \frac{\sum M_i x_i}{\sum M_N}$$

where M_i and x_i refer to the mass of atom i of BV and the position of BV atoms in the current snapshot, respectively, and M_N is the total mass of atoms of BV.

Results

PcyA variant assays

The previously reported enzyme activities for PcyA His74 variants utilized the gene product from the cyanobacterium *Nostoc* sp. PCC7120 PcyA locus [14]. In these studies, we examine PcyA from *Synechocystis* sp. PCC6803, which is 58.2% identical in amino acid sequence. Since *Synechocystis* PcyA also is three amino acids longer than the *Nostoc* enzyme, its residues are mostly numbered

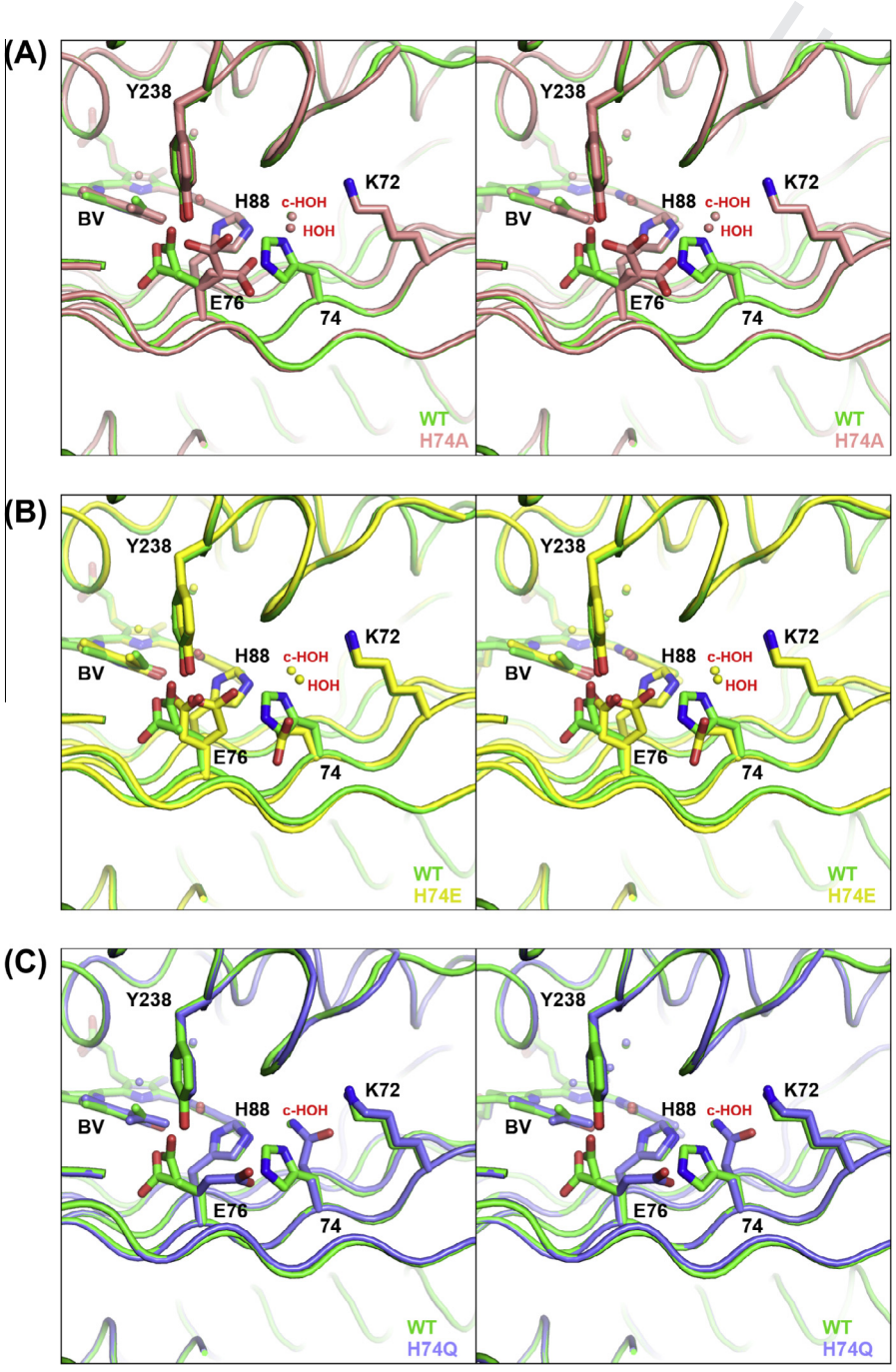


Fig. 2. Stereo superpositions of the PcyA His74 variants onto wild-type structure. Residues near position 74 are shown along with water molecules labeled HOH in red. The conserved water molecule between His88 and His74 observed in the wild-type structure is labeled 'c-HOH'. (A) H74A (salmon color) superposed onto wild type (green color). (B) H74E (yellow color) superposed onto wild type (green color). (C) H74Q (blue color) superposed onto wild type (green color). (For interpretation of the references to color in this figure legend, the reader is referred to the web version of this article.)

Please cite this article in press as: B. Kabasakal et al., Arch. Biochem. Biophys. (2013), http://dx.doi.org/10.1016/j.abb.2013.07.021

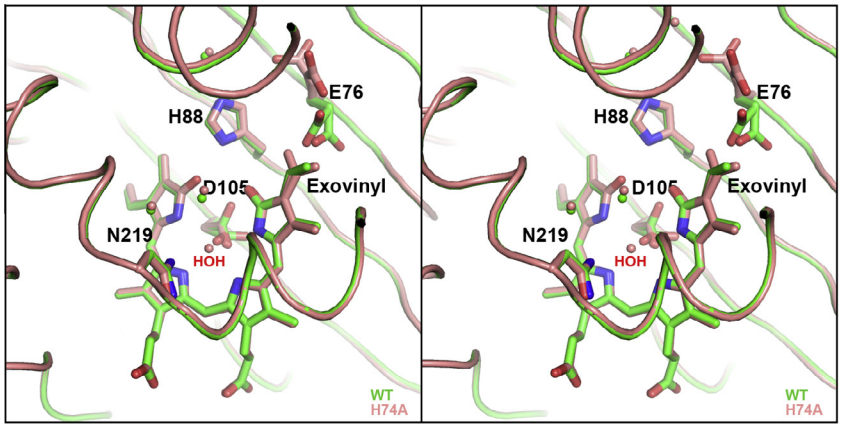


Fig. 3. Stereo superposition of the PcyA H74A active site onto wild type. Active site displayed with biliverdin bound showing the two conformations of the exovinyl group for the H74A variant. Also labeled in red is the water molecule that is centered above the four pyrrole nitrogens, which is not observed in the wild-type structure, but also seen in the H74Q and H74E structures as well as the D105 N and H88Q structures [13]. The same color scheme as in Fig. 1 is used. (For interpretation of the references to color in this figure legend, the reader is referred to the web version of this article.)

N + 3 compared to the previously published *Nostoc* enzyme. To confirm the consequences of the His74 variants in the *Synechocystis* enzyme, activity assays were conducted under the same experimental conditions used for the *Nostoc* enzyme. Wild type and variant PcyAs were incubated with ferredoxin, NADPH and ferredoxin:NADP$^+$ oxidoreductase (FNR) and BV substrate for 30 min under anaerobic conditions using an oxygen-scavenging system. Ten molar reducing equivalents of NADPH (compared to BV concentration) were added to ensure full BV reduction. Bilin products were quantitated by integrated peak area of HPLC runs (not shown) and percent conversion is given with respect to final PCB product observed for the wild-type enzyme [10]. As observed previously for the *Nostoc* PcyA variant, *Synechocystis* H74A was inactive. *Synechocystis* PcyA variants H74Q and H74E also exhibited activities similar to those of the *Nostoc* enzyme with 75% and 58% of the wild-type activity, respectively. These results suggest that the hydrogen-bonding properties and/or size of residue 74 are more important than its potential proton transfer capability. Alternatively, the side chain of residue 74 also may be needed to form a hydrogen bond to the bridging water with the catalytically important imidazole of His88.

PcyA variant structures

All three *Synechocystis* PcyA variants, H74A, H74E and H74Q, were crystallized in the dark with BV bound using sodium citrate as the precipitating agent. Large crystals were observed in about 1–2 weeks and data were collected on crystals frozen near liquid nitrogen temperatures. PcyA variants H74A, H74E and H74Q diffracted X-rays to 1.18, 1.30 and 1.49 Å resolution respectively, and each refined reasonably with respective *R*-factors of 14.9%, 16.5% and 17.9% and respective *R*-free values of 17.1%, 18.8% and 20.7%. Data collection and structure refinement statistics are given in Table 1. The overall folds of all three variants are essentially identical to PcyA wild type and superpose onto the wild-type structure with RMSDs of 0.292, 0.193 and 0.353 Å for the H74A, H74E and H74Q variants respectively (Table 1). PcyA adopts a three-layer α/β/α sandwich structure with a seven-stranded antiparallel β-sheet core and four helices stacked on both sides of the β-sheet center (Fig. 1). BV binds in a cyclic conformation between the β-sheet and C-terminal α-helices with the A- and D-rings buried in the protein core, and the propionate groups exposed to the surface.

Changes near residue 74

Comparing active sites of the H74A variant and wild-type PcyA revealed that the bridging water molecule between His88, His74 and Lys72 in wild-type PcyA is retained at a similar location in the H74A variant (Fig. 2A). An additional water molecule is present in the H74A variant that occupies the space vacated by the imidazole side chain of His74. This water molecule is situated very near the position vacated by Nδ1 of His74. The new water molecule forms an H-bond with Oε2 of Glu76, which also adopts two conformations, both of which shift towards the vacated space near Ala74 (Fig. 2A). These results indicate that the inactivity of the H74A variant is not due to the absence of a water molecule between the conserved residues His88 and Lys72, the latter previously proposed to be involved in proton transfer from the solvent and the substrate [12].

In contrast with the H74A variant, the H74E active site shows that Glu74 rotates away the conserved water molecule next to His88 (Fig. 2B). Surprisingly, a new bound water molecule is also present in the H74E variant in a similar location to the new water

Table 2
Atomic fluctuations (computed as RMSF) over the course of three molecular dynamics simulations carried out over 60 ns.

Residue	Root mean squared fluctuations (in Å)											
	Wild type Simulation			H74A Simulation			H74E Simulation			H74Q Simulation		
	1	2	3	1	2	3	1	2	3	1	2	3
BV	1.34	1.61	1.01	1.66	1.26	1.92	0.98	1.17	0.84	2.46	0.85	2.06
His88	0.70	1.02	0.70	0.92	0.75	0.83	0.55	0.61	0.51	0.98	0.98	1.02
Glu76	0.88	1.01	0.88	0.73	0.71	0.61	0.73	1.08	0.82	0.79	0.79	0.52
Asp105	0.59	0.63	0.59	0.74	0.49	0.91	0.67	0.50	0.39	0.62	0.62	0.59

UNCORRECTED PROOF

found in the H74A variant. This water lies close to the vacated atom Nδ1 ofHis74 present in wild-type PcyA. This water forms an H-bond with Oε2 of Glu74, but unlike H74A, it does not H-bond to Glu76 as this residue shifts more towards BV (and also resides in two conformations like the wild type and the H74A variant). Glu76 also makes a weak hydrogen bond (3.1 Å distance) with the main chain nitrogen of Arg63 in the neighboring β-strand. Given the 58% activity of H74E variant compared to the wild type, this newly placed water molecule apparently does not appear responsible for the loss of H74A activity.

Unexpectedly, the H74Q structure is the most different from those of the other two variants. In this regard, Gln74 lies between His88 and Lys72, displacing the conserved water molecule that normally lies in this position (Fig. 2C). The amide side chain of Gln74 is also H-bonded to His88 and Lys72 side chains, while the Nε2 atom of Gln74 lies at the same position of the water molecule normally seen in the other structures. It is interesting to note that the neutral amide group of Gln74 resides between His88 and Lys72 in the H74Q variant, while by contrast, the corresponding negatively charged Glu74 points away from residues His88 and Lys72 in H74E variant. This suggests that both His88 and Lys72 are uncharged. Previously, we have shown that His88 becomes deprotonated when bound to BV [13]. We suggest that Lys72 has a lower pK_a since it is buried and its amino group lies close (5.2 Å) to the positively charged guanidium group of Arg71. Unfortunately, the observed retention of activity of the H74Q variant is not obvious from its structure.

Changes in biliverdin and neighboring residues

All three variants adopt similar bound BV geometries (Figs. 2 and 3). In both the H74A and H74Q variants, Glu76 shifts away from the BV exovinyl group, resulting in two observable conformations for the D-ring exovinyl group (Fig. 3). The first of these is very similar to that seen in the wild type, while the 18^2 exovinyl carbon in the second points towards the other Glu76 conformation (Fig. 3). In the H74E structure, one of the Glu76 conformations places the carboxylic acid side-chain close to the vinyl group as in wild type, restricting the vinyl conformation to that of the wild-type enzyme (Fig. 2C). In all variants, two observable conformations are seen for Asp105, which are also observed for the wild type (Fig. 3). While previously we have argued that these two conformations account for the partial protonation of BV prior to the first electron reduction [9,13], the lack of a long-wavelength transition in the absorption spectra indicate that the protonated species is not favored in any of the H74 variants. Similarly, the conformation of His88 in all the variant structures is also identical with that of wild type (Figs. 2 and 3). Surprisingly, a new water molecule is seen in all variant structures, located within hydrogen bonding distance of all four pyrrole nitrogens and Asn219 (Fig. 3). This water molecule was also seen in the D105 N and H88Q variants – a water molecule shown to be lost upon radical formation [13]. This water molecule was hypothesized to stabilize BV binding in the H88Q/D105 N variant by H-bonding, since both variants are unable to protonate BV substrate. However, this water molecule

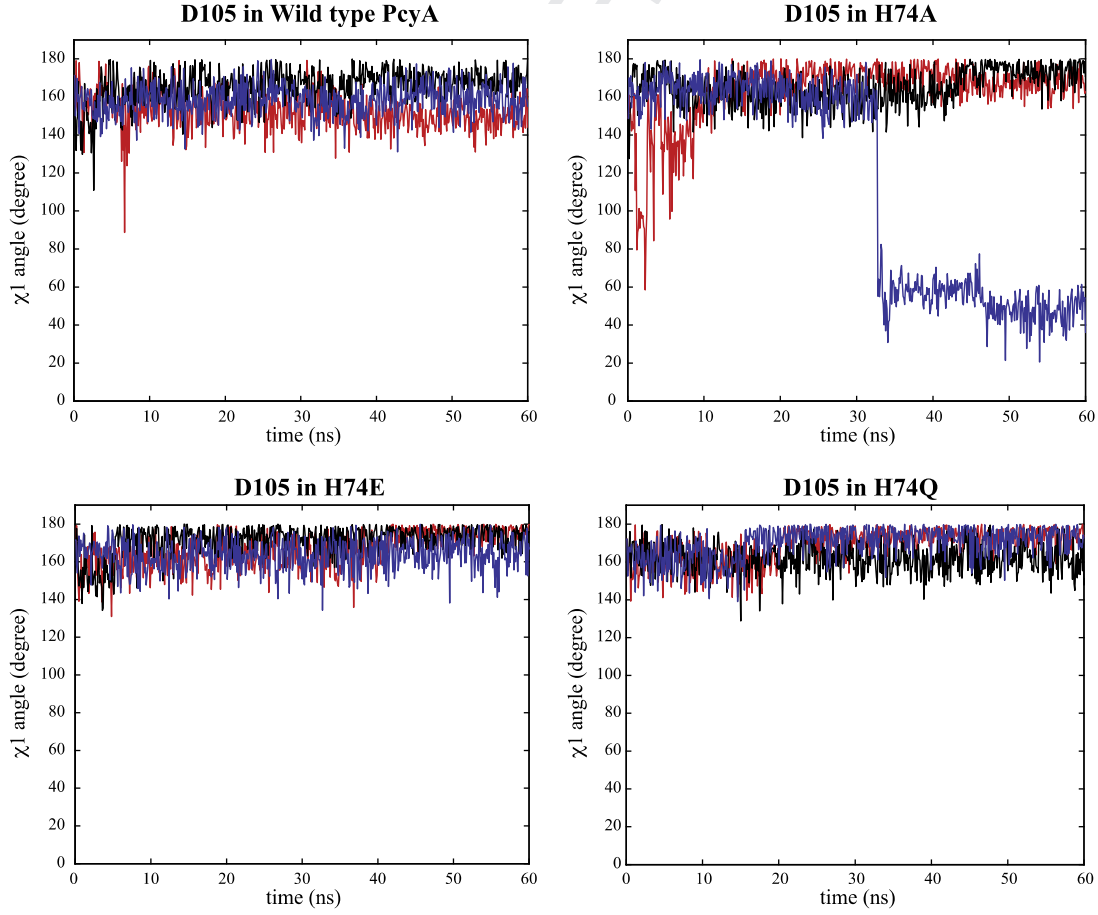


Fig. 4. The value of χ1 angle of Asp105 is plotted as a function of time. Note that the choice of colors for the three independent molecular dynamics simulations is consistent in this figure and in the subsequent Figs. 5 and 6.

may be able to bind because of increased dynamics and/or space at the BV binding site due to nearby variant perturbations.

Molecular dynamics simulations reveal differences in flexibility induced by mutations in PcyA

To assess the effects of the His74 mutations on the dynamics of the active site of PcyA, we carried out molecular dynamics simulations for the wild-type PcyA and the three His74 variants. Each simulation utilized the X-ray structure of each protein as initial conditions and was performed in the explicit presence of water and counter-ions to better approximate the active site environment. We ran three independent simulations of sixty nanoseconds for each protein, and snapshots were collected every 10 ps for analysis. We focused our analysis around the neighborhood of BV and His74 mutation in each of the BV-protein complexes (wild type, and the three H74 variants). For each complex, we computed the root mean square fluctuation (RMSF) of the protein atoms of Asp105, His88, Glu76, and BV substrate around the mean structures computed over the whole simulations. Results are shown in Table 2. The dynamics of His88 and Glu76 for the H74A, H74E and H74Q variants were similar to wild-type PcyA. In contrast, BV in the H74A and H74Q variants of BV fluctuated more substantially from their mean structures during the course of the simulation than wild type and H74E (Table 2). We also observed thatAsp105, a conserved residue in the active site of PcyA fluctuated more in the H74A variant compared to the three other proteins.

Interestingly, the increased dynamics of Asp105 is accompanied by an increase in the conformational space it can adopt in the active site. We monitored the $\chi 1$ angle of Asp105 over all three simulations, for all four proteins. Results are shown in Fig. 4. While the $\chi 1$ angle of Asp105 remained in a trans configuration in all simulations for wild-type PcyA, H74E, and H74Q, it was observed to switch to a gauche plus conformation in one of the simulations for H74A.

To measure the impact of the differential flexibilities of Asp105 in the four proteins on the stability of BV in the active site of PcyA, we computed the distance between Oδ1 of Asp105 and NC of BV (C-ring pyrrole Nitrogen) as a function of time. Results are shown in Fig. 5. For all four proteins, this distance is observed to oscillate between two states, one with a value of 3.2 Å, and the second one at 5.5 Å. Considering that Asp105 is relatively stable and remains in one rotameric state (see Fig. 4), this is consistent with two stable conformations of BV in the active site of PcyA. Interestingly however, in one of the three independent simulation trajectories for H74A we observe a significant increase in the distance between Oδ1 of Asp105 and NC of BV to approximately 8.0 Å, leading to a loss of interaction between Asp105 an the BV substrate. This loss if not observed in at least 180 ns of simulation for the other proteins.

Finally, we monitored the position of BV during the simulations for all four proteins. We computed the relative position of the center of gravity of BV for each complex with respect to its position in the corresponding X-ray structure and monitored this position as a function of time. Results are shown in

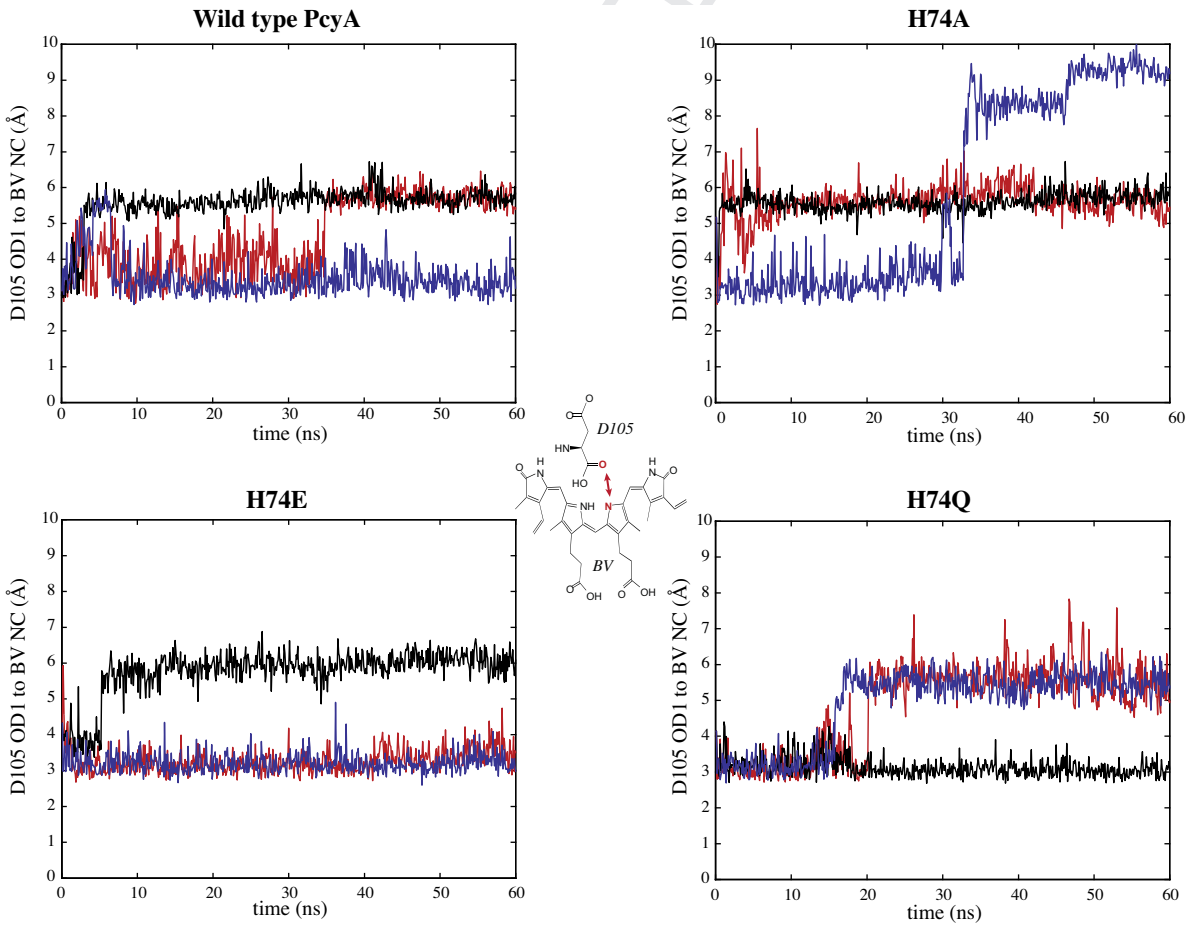


Fig. 5. The distance between Asp 105 Oδ1 and BV NC (C-ring pyrrole nitrogen) is plotted as a function of time during three independent molecular dynamics simulations for all four proteins under study. Three colors represent three different simulations.

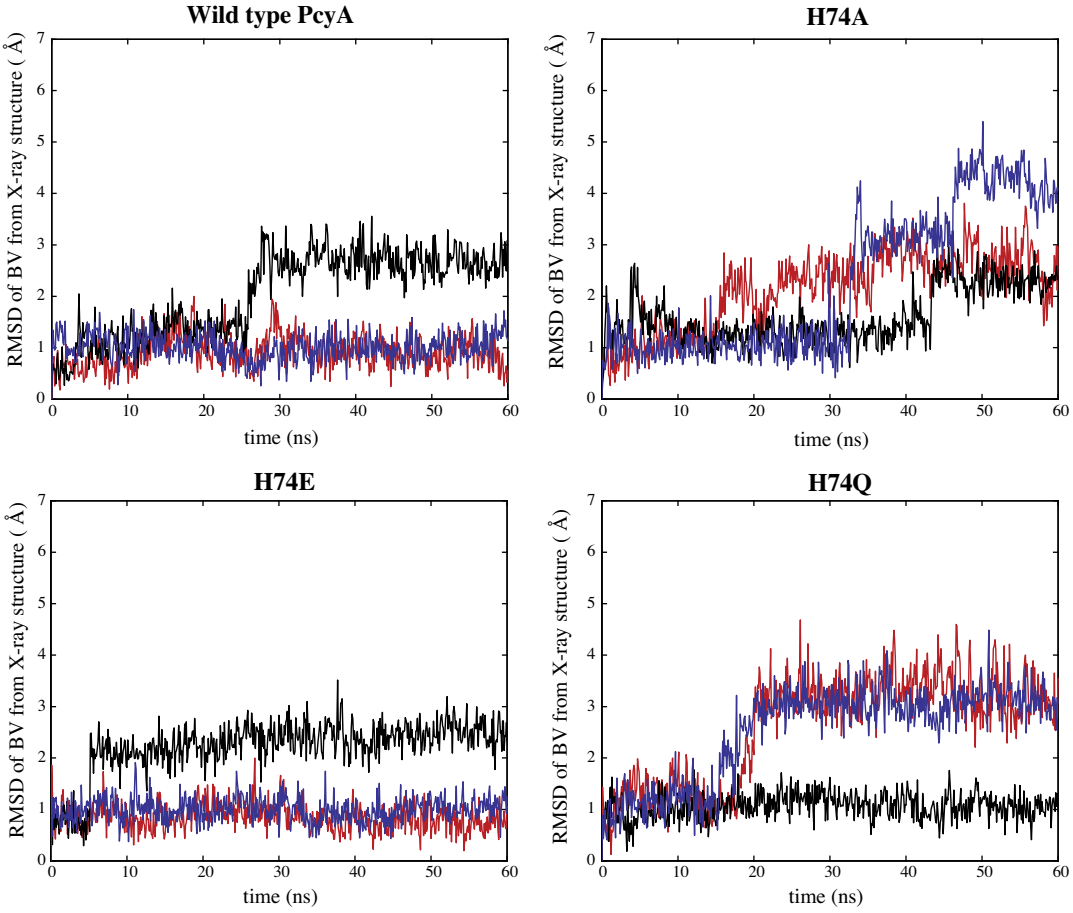


Fig. 6. The position of the center of gravity of BV is plotted as a function of time during three independent molecular dynamics simulations. Three colors represent three different simulations.

Fig. 6. In agreement with what we observed for the Asp105-BV distance, we observe that BV fluctuates between two conformations for most duplexes. In one simulation for the H74A mutant however, we observed BV to deviate monotonically from its position in the X-ray structure over the course of the simulation, ending more than 5 Å away. A movie of the simulation reveals that in this specific simulation, BV is leaving the active site (results not shown).

Discussion

PcyA is the most well characterized enzyme of the FDBR family – an enzyme that plays a critical role in the synthesis of the chromophores of photosensors involved in growth, development and energy harnessing in oxygenic photosynthetic organisms. A greater understanding of the mechanism of bilin reduction by FDBRs necessitates elucidation of the role of individual residues in their proton-coupled electron transfer function. These studies particularly probe the role of conserved residue His74. While fully conserved in the PcyA subfamily, this His residue is missing in FDBRs that catalyze the reduction of a single vinyl group such as PebA, PebB and HY2 [8]. Its conservation in PcyA suggests that it plays an important role in the four-electron reduction of two vinyl groups.

Here we confirm that the exchange of His74 to two other H-bonding residues similar in size has little effect on the activity of the *Synechocystis* enzyme, while alanine substitution yields an inactive enzyme. These results are consistent with the measured activities of same variants of *Nostoc* PcyA [14]. This argues that His74 does not directly participate in proton transfer, but is plays a key role in positioning potential proton donors. The crystal structure of PcyA revealed that His74 forms a hydrogen bond with a buried water molecule, which in turn interacts with the catalytically important His88 [11,12]. We previously hypothesized that this water molecule plays a key role in the re-protonation of His88 for catalytic turnover.

In the present work, we report the high-resolution crystal structures of three His74 variants; H74A, H74E and H74Q. These structures reveal that while the buried water molecule is retained in the H74A and H74E variants, this bridging water is dislodged by the amide group of Gln74 in the H74Q variant. This water molecule is therefore non-essential for activity as we show that the H74Q variant still retained 75% activity. Molecular dynamics simulations also show that changes in His74 do not alter the mobility of nearby Glu76 which could account for the loss of activity for the H74A variant.

So why is the H74A variant inactive? Based on these comparative analyses, the reasons for the loss of activity of the H74A variant cannot be ascribed to changes in structure so it is likely that differences in dynamics are responsible. Based on three independent molecular dynamics simulations, we observed that the H74A differed from the other mutants (H74Q and H74E) and from the wild-type proteins by two characteristics. Not only is Asp105 much more dynamic in H74A compared with the other complexes but one of the simulations revealed that BV was able to escape the

active site only for theH74A variant. Both observations are consistent with a reduced affinity of BV with the active site of the H74A variant. This strongly suggests that residue 74 stabilizes the orientation(s) of the side chain of Asp105 that is essential for activity [14], likely via hydrogen bonding interactions with BV, to enable proton-coupled electron transfer prior to release of the substrate and/or the semi-reduced intermediate. The H74A variant may also possess a reduced midpoint potential that may be influenced by the altered positioning of water molecules that function as proton donors at the active site. Experiments to assess the rates of substrate binding and dissociation to the wild type and PcyA variants, in combination with electrochemical measurements, will be required to address these issues.

Acknowledgments

This work was supported in part by National Science Foundation Grant MCB-0843625 to A.J.F. and J.C.L. A National Institutes of Health training grant T32-GM007377 supported D.D.G. Portions of this research were carried out at the Stanford Synchrotron Radiation Lightsource, a national user facility operated by Stanford University on behalf of the U.S. Department of Energy, Office of Basic Energy Sciences. The SSRL Structural Molecular Biology Program is supported by the Department of Energy, Office of Biological and Environmental Research, and by the National Institutes of Health, National Center for Research Resources, Biomedical Technology Program, and the National Institute of General Medical Sciences.

References

[1] S.I. Beale, Chem. Rev. 93 (1993) 785–802.
[2] N.F. Frankenberg, J.C. Lagarias, in: R. Guilard (Ed.), The Porphyrin Handbook. Chlorophylls and Bilins: Biosynthesis Structure and Degradation, Academic Press, New York, 2003, pp. 211–235.
[3] N. Rockwell, Y. Su, J. Lagarias, Annu. Rev. Plant Biol. (2006).
[4] R.A. Sharrock, Genome Biol. 9 (2008) 230.
[5] E. Schäfer, F. Nagy (Eds.), Photomorphogenesis in Plants and Bacteria: Function and Signal Transduction Mechanisms, third ed., Springer, Dordrecht, The Netherlands, 2005.
[6] L.N. Duysens, Nature 168 (1951) 548–550.
[7] A.N. Glazer, Annu. Rev. Biophys. Biophys. Chem. 14 (1985) 47–77.
[8] N. Frankenberg, K. Mukougawa, T. Kohchi, J. Lagarias, Plant Cell 13 (2001) 965–978.
[9] S.L. Tu, A. Gunn, M.D. Toney, R.D. Britt, J.C. Lagarias, J. Am. Chem. Soc. 126 (2004) 8682–8693.
[10] N. Frankenberg, J.C. Lagarias, J. Biol. Chem. 278 (2003) 9219–9226.
[11] Y. Hagiwara, M. Sugishima, Y. Takahashi, K. Fukuyama, Proc. Natl. Acad. Sci. USA 103 (2006) 27–32.
[12] S.-L. Tu, N.C. Rockwell, J.C. Lagarias, A.J. Fisher, Biochemistry 46 (2007) 1484–1494.
[13] A.C. Kohler, D.D. Gae, M.A. Richley, S. Stoll, A. Gunn, S. Lim, S.S. Martin, T.I. Doukov, R.D. Britt, J.B. Ames, J.C. Lagarias, A.J. Fisher, Biochemistry 49 (2010) 6206–6218.
[14] S.L. Tu, W. Sughrue, R.D. Britt, J.C. Lagarias, J. Biol. Chem. 281 (2006) 3127–3136.
[15] Y. Hagiwara, M. Sugishima, Y. Takahashi, K. Fukuyama, FEBS Lett. 580 (2006) 3823–3828.
[16] S. Stoll, A. Gunn, M. Brynda, W. Sughrue, A.C. Kohler, A. Ozarowski, A.J. Fisher, J.C. Lagarias, R.D. Britt, J. Am. Chem. Soc. 131 (2009) 1986–1995.
[17] T.D. Elich, A.F. McDonagh, L.A. Palma, J.C. Lagarias, J. Biol. Chem. 264 (1989) 183–189.
[18] T.G. Battye, L. Kontogiannis, O. Johnson, H.R. Powell, A.G. Leslie, Acta Crystallogr. D Biol. Crystallogr. 67 (2011) 271–281.
[19] W. Kabsch, Acta Crystallogr. D Biol. Crystallogr. 66 (2010) 125–132.
[20] A. McCoy, Acta Crystallogr. D Biol. Crystallogr. 63 (2007) 32–41.
[21] G.N. Murshudov, P. Skubak, A.A. Lebedev, N.S. Pannu, R.A. Steiner, R.A. Nicholls, M.D. Winn, F. Long, A.A. Vagin, Acta Crystallogr. D Biol. Crystallogr. 67 (2011) 355–367.
[22] P. Emsley, K. Cowtan, Acta Crystallogr. D Biol. Crystallogr. 60 (2004) 2126–2132.
[23] Y. Hagiwara, M. Sugishima, H. Khawn, H. Kinoshita, K. Inomata, L. Shang, J.C. Lagarias, Y. Takahashi, K. Fukuyama, J. Biol. Chem. 285 (2010) 1000–1007.
[24] V. Hornak, R. Abel, A. Okur, B. Strockbine, A. Roitberg, C. Simmerling, Proteins 65 (2006) 712–725.
[25] J. Wang, R.M. Wolf, J.W. Caldwell, P.A. Kollman, D.A. Case, J. Comput. Chem. 25 (2004) 1157–1174.
[26] J. Wang, W. Wang, P.A. Kollman, D.A. Case, J. Mol. Graph Model 25 (2006) 247–260.
[27] A. Jakalian, D.B. Jack, C.I. Bayly, J. Comput. Chem. 23 (2002) 1623–1641.
[28] D.A. Case, T.E. Cheatham 3rd, T. Darden, H. Gohlke, R. Luo, K.M. Merz Jr., A. Onufriev, C. Simmerling, B. Wang, R.J. Woods, J. Comput. Chem. 26 (2005) 1668–1688.
[29] J.C. Phillips, R. Braun, W. Wang, J. Gumbart, E. Tajkhorshid, E. Villa, C. Chipot, R.D. Skeel, L. Kale, K. Schulten, J. Comput. Chem. 26 (2005) 1781–1802.
[30] H.J. Berendsen, J.P. Postma, W.F. van Gunsteren, A. Di Nola, J.R. Haak, J. Chem. Phys. 81 (1984) 3684–3690.
[31] T. Darden, D. York, L. Pedersen, J. Chem. Phys. 98 (1993) 10089–10092.

UNCORRECTED PROOF